

Dynamics of Charge Carriers in Silicon Nanowire Photoconductors Revealed by Photo Hall Effect Measurements

Kaixiang Chen,[†] Xiaolong Zhao,[‡] Abdelmadjid Mesli,[§] Yongning He,^{*,‡} and Yaping Dan^{*,†,‡,§}

[†]State Key Laboratory of Advanced Optical Communication Systems and Networks, University of Michigan-Shanghai Jiao Tong University Joint Institute, Shanghai Jiao Tong University, 800 Dong Chuan Road, Shanghai 200240, China

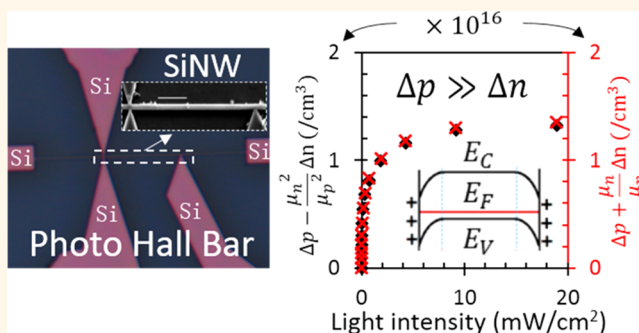
[‡]School of Microelectronics, Xi'an Jiao Tong University, 28 Xian Ning Road, Xi'an, Shaanxi Province 710049, China

[§]Institut Matériaux Microélectronique Nanosciences de Provence, UMR 6242 CNRS, Université Aix-Marseille, 13397 Marseille Cedex 20, France

Supporting Information

ABSTRACT: Photoconductors have extraordinarily high gain in quantum efficiency, but the origin of the gain has remained in dispute for decades. In this work, we employ photo Hall effect to reveal the gain mechanisms by probing the dynamics of photogenerated charge carriers in silicon nanowire photoconductors. The results reveal that a large number of photogenerated minority electrons are localized in the surface depletion region and surface trap states. The same number of excess hole counterparts is left in the nanowire conduction channel, resulting in the fact that excess holes outnumber the excess electrons in the nanowire conduction channel by orders of magnitude. The accumulation of the excess holes broadens the conduction channel by narrowing down the depletion region, which leads to the experimentally observed high photo gain.

KEYWORDS: silicon nanowire, photoconductor, gain mechanism, photo Hall effect, surface states



Photoconductors are often reported to have high gain in quantum efficiency (up to 10^8).^{1–3} It is commonly believed that the high gain originates from the circulation of photogenerated carriers in the circuit many times before they recombine.⁴ The theoretical foundation of this gain mechanism was developed in 1950s.⁵ It shows that the gain G is equal to the minority carrier lifetime τ_m divided by the transit time τ_t that carriers take to transport from one electrode to the other, that is, $G = \tau_m/\tau_t$ or similar forms. However, the experimentally measured gain is often reported to be inconsistent with the theoretical prediction. For example, Matsuo *et al.*⁶ found in 1984 that the measured gain in GaAs thin-film photoconductors is larger than the theoretical prediction by 3–4 orders of magnitude. Due to this reason, Zardas *et al.*⁷ believe that the minority carrier lifetime is actually longer because of the separation of electron–hole pairs by the depletion region near the semiconductor surfaces. Konstantatos *et al.*⁸ simply replaced the short minority carrier lifetime with the long trap lifetime to explain away the phenomena. Unfortunately, the original theory does not support this claim. Other researchers believe that the classical gain mechanism is somewhat problematic, and they are actively

searching for new gain mechanisms. In late 1990s, Munoz *et al.*^{9,10} proposed with simulations that the photoconductive gain comes from the photo modulation of the depletion region width near the photoconductor surfaces. In 2005, Calarco *et al.*¹¹ observed the size-dependent photoconductivity in GaN nanowires and proposed a surface electron–hole pair recombination model to describe the unusual persistent photocurrents in the nanowires. Several years later, Kim *et al.*¹² investigated the diameter-dependent photogain of Ge nanowires and interpreted that the gain originates from the surface photogating effects of trapped electrons at the nanowire surfaces. In 2014, Furchi *et al.*¹³ studied the photoconductivity in atomically thin MoS₂ monolayers and found that both the photovoltaic and photoconductive effects contribute to the photogain. All these proposed gain models can explain most if not all of the observed phenomena either quantitatively or qualitatively. But the photoconductor devices remain more like

Received: January 1, 2018

Accepted: March 19, 2018

Published: March 19, 2018

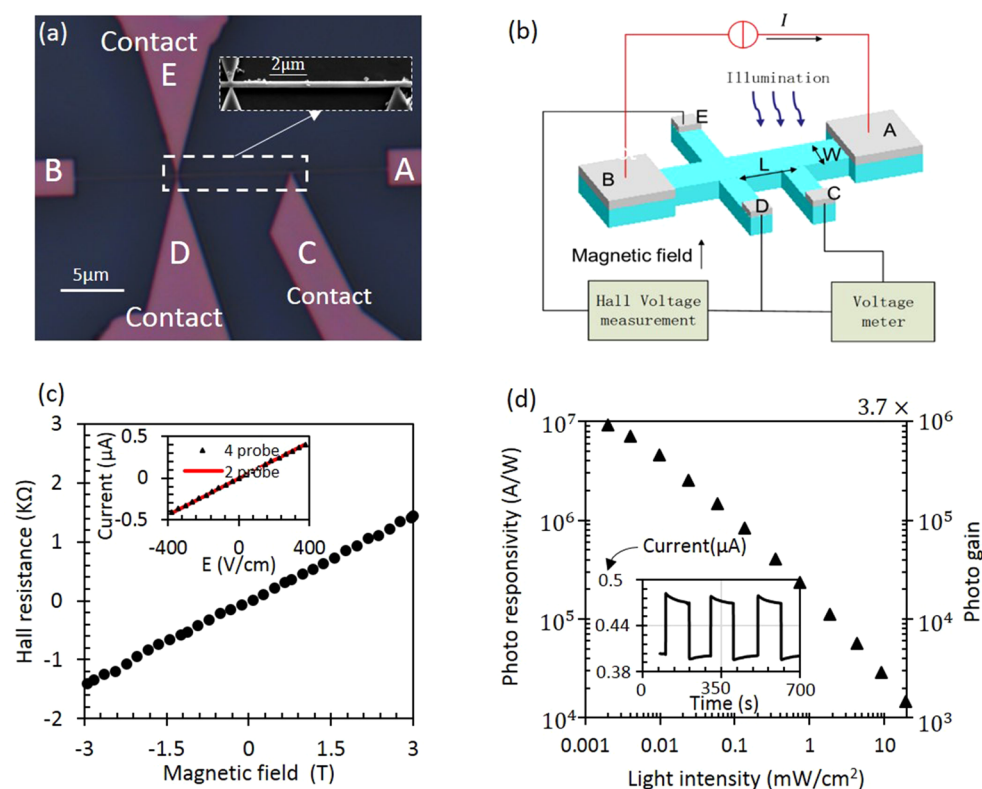


Figure 1. (a) Optical microscopic image of a typical SiNW photoconductor with Hall bar geometry. Inset: SEM image of the SiNW. (b) Schematic illustration of experimental setup and device structure. The device is biased between A and B electrodes, while the handling substrate is floating. (c) Hall resistance as a function of magnetic field intensity in the dark. Inset: Current vs Electric field (E) for four- and two-probe measurements. (d) Photoresponsivity and photogain vs light illumination intensity (the device is biased at 3 V). Inset: Transient current as light illumination (19 mW/cm^2) is periodically switched on/off (accordingly high/low in current biased at 1 V).

a black box. It is difficult to provide a definite answer unless what is happening inside the photoconductor can be revealed.

In this work, we employed photo Hall effect to better understand the dynamics of photogenerated charge carriers in silicon nanowire photoconductors. The experimental data show that the p-type nanowires are partially depleted in the dark due to surface charges. The information on the depletion region allows us to accurately estimate the doping concentration, hole mobility, and excess hole concentration of the nanowire. Under light illumination, a large number of photogenerated minority electrons are localized in the surface depletion region and surface trap states. The same number of excess hole counterparts is accumulated in the nanowire conduction channel, resulting in the fact that excess holes outnumber the excess electrons in the nanowire conduction channel by orders of magnitude. The accumulation of the excess holes broadens the conduction channel width by narrowing down the depletion region, which leads to the experimentally observed high photo gain.

RESULTS AND DISCUSSION

The nanowires were fabricated by patterning the device layer of a silicon-on-insulator (SOI) wafer with electron beam lithography, reactive ion etch, and metal evaporation. The device layer is p-type with a doping concentration of $\sim 10^{17} \text{ cm}^{-3}$. The large contact silicon micropads were p-type doped at high concentration ($\sim 5 \times 10^{18} \text{ cm}^{-3}$) to facilitate the formation of ohmic contacts. The device layer started with a thickness of 220 nm but was thinned down to 210 nm after wet oxidation

and cleaning process. The thickness of the SiO_2 insulating layer is $2 \mu\text{m}$. As a result, any possible photo gating effect can be neglected, although the handling substrate is electrically floating. Figure 1a shows the optical microscopic image of such a single silicon nanowire device. A close-up scanning electron microscopic (SEM) image of the nanowire is shown in the inset. The Hall bar geometry is all made of silicon, and metal electrodes are only in contact with the Si micropads (Figure 1b). Four probe and photo Hall effect measurements were conducted in a physical property measurement system (PPMS Evercool-II). The Hall resistance is linearly dependent on the magnetic field intensity (Figure 1c). The two- and four-probe measurements provide nearly identical linear current vs electric field curves (inset of Figure 1c), indicating that the Si pads are in ohmic contact with metal electrodes and the contact resistances are negligibly small. Under light illumination ($\lambda = 460 \text{ nm}$), the photoconductance of the nanowire quickly ramps up and is then followed by a small decay (inset of Figure 1d). The nanowire photoresponsivity is as high as 10^6 A/W at low light intensity and decreases to 10^4 A/W at 20 mW/cm^2 . Accordingly, the gain in quantum efficiency of the nanowire photoconductor ranges from 10^3 to 10^6 , as shown in Figure 1d (see SI Section 1 for calculations). Similar observations have been widely reported in literature.^{14–16}

To find the origin of the high photo gain, we need to reveal the dynamics of photogenerated charge carriers inside the nanowire. Under light illumination, the concentration of excess charge carriers can be derived from photoconductance as expressed in eq 1:

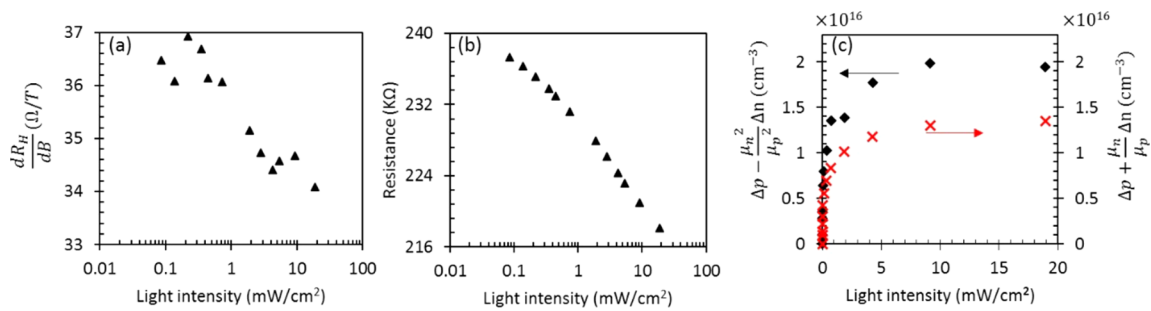


Figure 2. (a) Derivative of Hall resistance respective to magnetic field (dR_H/dB), (b) nanowire resistance, (c) $\Delta p - \frac{\mu_n^2}{\mu_p^2} \Delta n$ and $\Delta p + \frac{\mu_n}{\mu_p} \Delta n$ as light illumination intensity increases.

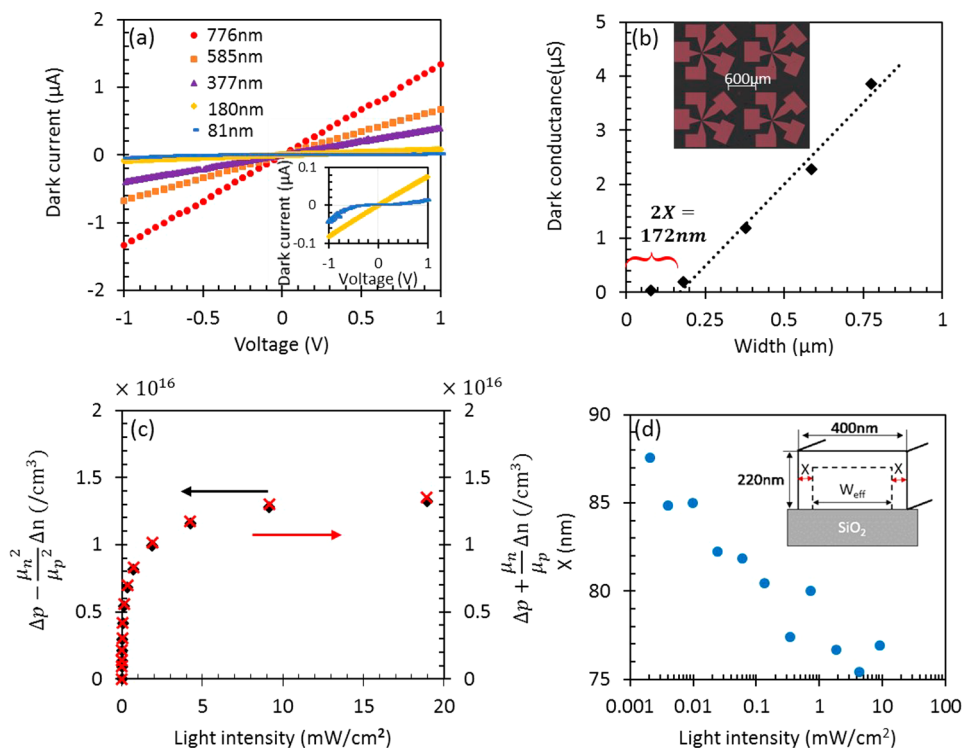


Figure 3. (a) Current–voltage (I – V) curve for SiNWs from 81 to 776 nm in width. (b) Nanowire conductance as a function of wire width in the dark. (c) Experimental data of $\Delta p - \frac{\mu_n^2}{\mu_p^2} \Delta n$ and $\Delta p + \frac{\mu_n}{\mu_p} \Delta n$ for the SiNW ($\sim 10^{17}$ cm⁻³, 377 nm width) after the depletion region width is taken into account. (d) Depletion region width modulated by light illumination. Inset: Sketch of conduction channel and depletion region in the nanowire cross-section.

$$\Delta p + \frac{\mu_n}{\mu_p} \Delta n = \frac{L}{e\mu_p W t} \times \left(\frac{1}{R} - \frac{1}{R_0} \right) \quad (1)$$

where μ_n and μ_p are the electron and hole mobility, Δn and Δp are the excess electron and hole concentration, R_0 and R are the nanowire resistance in the dark and under light illumination, respectively, e is the unit charge, and W , L , and t are the nanowire physical width, length, and thickness, respectively. The concentration of excess charge carriers can also be found from photo Hall effect measurements which is governed by eq 2 (see SI Section 2 for the equation derivation):

$$\Delta p - \frac{\mu_n^2}{\mu_p^2} \Delta n = \frac{L^2}{e\mu_p^2 W^2 t} \times \left(\frac{dR_H/dB}{R^2} - \frac{dR_{H0}/dB}{R_0^2} \right) \quad (2)$$

where R_0 , R_{H0} , R , and R_H are the nanowire resistance and Hall resistance in the dark and under light illumination, respectively. The derivative of Hall resistance with respect to magnetic field dR_H/dB is the slope of the linear dotted line in Figure 1c. This derivative at different light intensity is shown in Figure 2a. The nanowire resistance R extracted from I – V curves was experimentally monitored as the light intensity increases (Figure 2b). The right side of both eqs 1 and 2 are the experimentally measured data, and the left sides are inferred parameters. These inferred parameters are plotted as a function of light illumination intensity, shown in Figure 2c where the red crosses are found from eq 1 and the black diamonds from eq 2.

The data points in Figure 2c exhibit a number of unexpected characteristics. First, $\Delta p - \frac{\mu_n^2}{\mu_p^2} \Delta n$ (black diamonds) is clearly larger than $\Delta p + \frac{\mu_n}{\mu_p} \Delta n$ (red crosses), although mathematically

the former must always be smaller than the latter. Second, for the case of an intrinsic semiconductor, we expect that the term $\Delta p - \frac{\mu_n^2}{\mu_p^2} \Delta n$ would be negative since electrons in silicon have a mobility ~ 3 times larger than holes,⁴ like what we observed in a surface passivated bulk silicon photoconductor (see SI Section 3). However, we find a positive $\Delta p - \frac{\mu_n^2}{\mu_p^2} \Delta n$, which implies that

Δp is at least 9 times higher than Δn , although the electrons and holes are excited in pairs. These unexpected observations lead us to conclude that some factor was neglected in the calculations, causing a systematic error in the estimation of excess charge carrier concentration.

We believe that the neglected factor might be the depletion region near the nanowire surfaces due to surface charges. The existence of depletion region will lead to an overestimation of the actual width and thickness of the nanowire conduction channel when the nanowire physical dimensions are used for calculation. As a consequence, the terms $\Delta p - \frac{\mu_n^2}{\mu_p^2} \Delta n$ and

$\Delta p + \frac{\mu_n}{\mu_p} \Delta n$ in Figure 2c will be over or underestimated to different extents, resulting in those unexpected observations. To verify the existence of the depletion region in the nanowire, we measured the dark current–voltage (I – V) characteristics (also see SI Section 4 for photocurrent characteristics) for an array of silicon nanowires fabricated on the same chip ranging from ~ 81 nm to ~ 776 nm. The I – V characteristics are all linear except for the 81 nm wide nanowire (inset of Figure 3a). When the nanowire conductance in the dark is plotted against the nanowire width, we find that the nanowire conductance linearly decreases as the nanowire narrows down, except for the 81 nm wide nanowire which clearly deviates from this trend. This means that the 81 nm nanowire is somehow substantially different from the other wires, although all the wires went through exactly the same processes. The data points excluding the 81 nm wire can be fitted into a linear dashed line. The intercept of the line at x -coordinate is 172 ± 34 nm (Figure 3b). This means that a nanowire narrower than 172 ± 34 nm will be fully depleted. Since the depletion region exists at both side surfaces of the nanowire, the actual depletion region near the nanowire surfaces will be approximately 86 ± 17 nm wide. Note that the nanowires are patterned out of the device layer of an SOI wafer. SOI wafers have a high-quality Si–SiO₂ interface on which the concentration of static charges is normally small. It is fair to assume that no depletion region exists near this interface. Based on this assumption, the actual thickness of the channel will be ~ 124 nm ($= 210 - 86$), after deducting the depletion region width near the top nanowire surface.

A 377 nm-wide nanowire that has a total depletion region of 172 nm will result in an overestimation as much as 75% in channel width and height. This leads to a significant error in the estimation of doping concentration, carrier mobility, and the concentration of photogenerated majority charge carriers, as shown in Table 1 (see SI Section 2 for the calculation equations).

After we replace the nanowire physical width with the effective channel width and update other parameters in eqs 1 and 2, the two terms $\Delta p - \frac{\mu_n^2}{\mu_p^2} \Delta n$ and $\Delta p + \frac{\mu_n}{\mu_p} \Delta n$ are nearly identical at all light intensities as shown in Figure 3c. For highly doped silicon nanowires ($\sim 10^{18}$ cm⁻³), the depletion region is

Table 1. Measured Parameters before and after the Depletion Region Is Taken into Account

	physical width ($W = 377$ nm)	effective channel width ($W_{\text{eff}} = 205$ nm)
doping concentration p_0	6.3×10^{16} cm ⁻³	1.06×10^{17} cm ⁻³
hole mobility μ_p	130 cm ² /(V s)	240 cm ² /(V s)
excess hole concentration Δp at 20 mW/cm ²	1.9×10^{16} cm ⁻³	1.35×10^{16} cm ⁻³

much smaller. The actual channel width is approximately equal to the nanowire physical width. The measured $\Delta p - \frac{\mu_n^2}{\mu_p^2} \Delta n$ and $\Delta p + \frac{\mu_n}{\mu_p} \Delta n$ are almost identical without taking into account the depletion region width (see SI Section 5 for the experimental data).

The fact that the two terms $\Delta p - \frac{\mu_n^2}{\mu_p^2} \Delta n$ and $\Delta p + \frac{\mu_n}{\mu_p} \Delta n$ are nearly identical means that the concentration (more accurately the total number) of excess holes in the conduction channel is orders of magnitude higher than that of the excess electrons, although excess electrons and holes are generated in pairs by light illumination. The accumulation of excess holes and the deficit of excess electrons in the channel are caused by the localization of excess electrons at surface states and within surface depletion region. Indeed, after the nanowire devices are surface passivated by molecular monolayers, the photoresponse is significantly reduced (also see our recent publication),¹⁷ resulting in a much smaller gain or even no gain at all, although the minority carrier lifetime becomes longer (higher excess minority concentration).¹⁸ The reduced photoresponse leads to no detectable photo Hall signals in experiments (data not shown here). The further validation of the role of surface states and fixed charges by simulations will be presented later.

The physical separation of photogenerated electrons (near surfaces) and holes (in the channel) will induce an electric field perpendicular to the nanowire channel, resulting in the photo modulation of the actual channel width. As shown in Figure 3d, the depletion region width narrows down from 86 to 76 nm (actual channel width expands from 205 to 225 nm) as the light intensity increases to 10 mW/cm². Although the channel width expands by only ~ 20 nm, a large number of fixed dopant ions (20 nm \times 1.07×10^{17} cm⁻³ \times 124 nm) in the depletion region are neutralized by the excess holes accumulated in the channel. Our experimental data show that the excess hole concentration drops by at least 1 order of magnitude to reach a value lower than 10^{15} cm⁻³ after the channel expands (see SI Section 6). In short, the photo gain is caused by the accumulation of photogenerated majority carriers in the nanowire conduction channel that are orders of magnitude higher in number than the excess minority carriers. Most of the accumulated excess carriers move to neutralize the dopant ions in the depletion region, as a result of which the depletion region narrows down and the channel width expands. The remaining small fraction of the excess majority charge carriers leads to only a moderate increase in majority carrier concentration. This picture is consistent with the previous simulation results.⁹

Given that the p-type Si nanowire has a doping concentration of 1.06×10^{17} cm⁻³ and a surface depletion layer 86 nm wide, we conclude that the nanowire surfaces have positive charges with a concentration of 8.9×10^{11} cm⁻² by using the Silvaco Atlas Simulator. The surface charges will bend

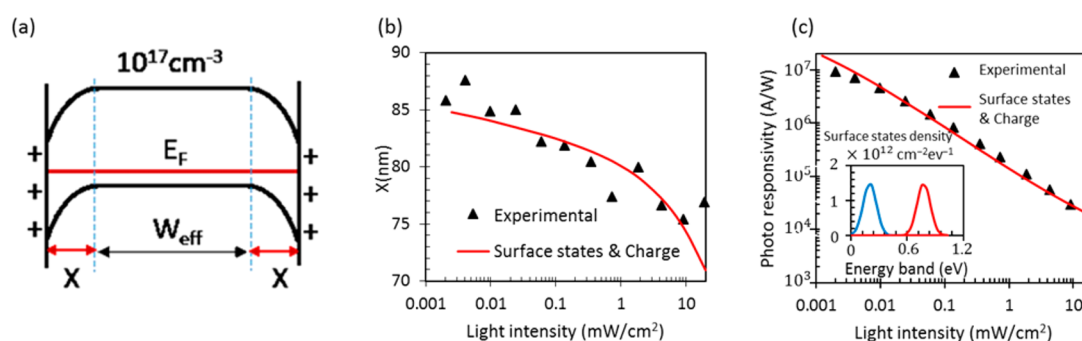


Figure 4. (a) Energy band diagram with net surface charges of $8.9 \times 10^{11} \text{ cm}^{-2}$. (b) Depletion region width and (c) photoresponsivity as a function of light illumination intensity. Inset in panel c: Density of surface states in the silicon bandgap in which the red profile is the acceptor-type states in the upper half bandgap and the blue profile is the donor-type states in the lower half bandgap. The fixed charges ($9.0 \times 10^{11} \text{ cm}^{-2}$) are uniformly distributed.

down the energy band by $\sim 0.6 \text{ eV}$ from the nanowire bulk to surfaces (Figure 4a). The surface charges may originate from fixed charges (for example, Na^+ or H^+ ionic charges). However, we found that the nanowire photoresponse with the presence of only fixed charges on surfaces is much smaller than our experimental data (see SI Section 7 for more discussions). In the following simulations, we added surface states in addition to fixed charges. Let us suppose that surface states have a distribution profile in silicon bandgap as shown in the inset of Figure 4c, which is typical for Si– SiO_2 interface.¹⁹ The net surface charges can still remain the same as $8.9 \times 10^{11} \text{ cm}^{-2}$ if we properly choose the density of fixed charges and surface states. In this case, the calculated channel width modulation and photoresponsivity can fit well with the experimental data (Figure 4b,c). It is worth pointing out that surface states can efficiently capture a large number of photoexcited minority charge carriers under the condition that majority charge carriers near surfaces are depleted by energy band bending. Otherwise, excess electrons in the surface states will effectively recombine with the majority holes, turning the surface states into efficient recombination centers instead of trap states.

To further validate the role of surface states in the photo gain, we also measured the frequency dependence of the nanowire photoresponse under the illumination of chopped light (20 mW/cm^2). As shown in Figure 5, the 3 dB bandwidth of our 377 nm-wide nanowire photoconductor is only $\sim 50 \text{ Hz}$

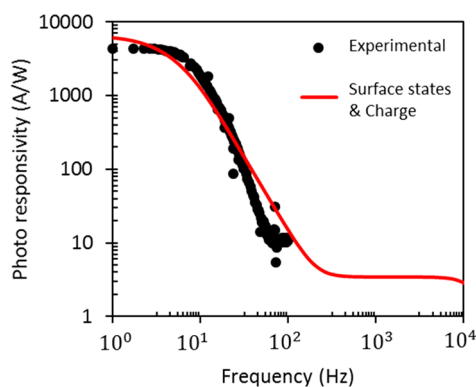


Figure 5. Frequency response of the nanowire photoconductor under periodic light excitation. The SiNW is 377 nm wide and the p-type doping concentration is $1.07 \times 10^{17} \text{ cm}^{-3}$. Experimental and simulation data are plotted in black dots and red line, respectively. The modulated light illumination intensity is 19 mW/cm^2 .

due to the long emission lifetime of surface trap states, which is often reported in literature.^{10,13,20,21} The simulated frequency-dependent photoresponsivity (red line in Figure 5) for the nanowire with the specified surface state density (inset in Figure 4c) and fixed charges can largely fit the experimental results (black dots). The inconsistency mainly originates from the fact that we can only assign a single value of capture cross-section to all surface states due to the limitation of the Silvaco software (but surface states at different energy levels have different capture cross sections). In contrast, if there are no surface states but only fixed charges on the nanowire surfaces, the photoresponsivity at low frequencies is about 1 order of magnitude lower and the 3 dB bandwidth will be as wide as hundreds of kHz (see SI Section 7 for the frequency response). Interestingly, the results indicate that a high-gain and wide-bandwidth photoconductor can be made if the nanowires are well surface-passivated but depleted by fixed charges on the surfaces (by metal gate, for example).²² Surface states can further increase the gain of nanoscale photoconductors but significantly reduce the 3 dB bandwidth to tens of hertz or even lower. Note that the existence of surface states in the bandgap of silicon can extend the sensitive spectral response of the nanowire photoconductor beyond the absorption edge of silicon (see SI Section 8 for the spectral response). The surface-states-induced high gain Si nanoscale photoconductors may find important applications in infrared photo detection when high speed is not required.

CONCLUSIONS

In conclusion, photo Hall effect measurements in this work were employed to investigate the dynamics of photogenerated excess carriers in silicon nanowires. The results show that the nanowires are partially depleted due to surface states and surface fixed charges. The depletion region width is quantitatively measured, which allows us to find the correct value of carrier mobility, doping concentration, and excess carrier concentration. The data further indicate that a large number of photogenerated minority carriers are localized by the surface depletion region and surface states. The same number of excess majority counterparts is left in the nanowire conduction channel, contributing to the widely observed photo gain. This work helps resolve the dispute on the origin of high photo gain in nanoscale photoconductors and may guide researchers to design high-performance photoconductors.

METHODS

The SOI device layer is doped with boron dopants by ion implantation. Electron beam lithography and reactive ion etch (RIE) process followed by Al thermal evaporation were then employed to define the Al etching mask for the nanowire Hall bar geometry with contact micropads. To obtain ohmic contacts, we highly doped ($5 \times 10^{18} \text{ cm}^{-3}$) the Si micropads. Photolithography and thermal evaporation of Al (270 nm thick) were performed to make electrical contacts to the silicon micropads of the devices. The SiNWs with a low doping concentration were treated with oxygen plasma to tune the surface quality. After photo Hall effect measurements, we used SEM to measure the physical width of the SiNWs before and after SiO₂ on the SiNW surfaces was removed by HF.

The photo Hall effect experiments were conducted in a physical property measurement system (PPMS, Quantum Design Inc.) in which we installed an LED with the central peak wavelength at 460 nm and the full width at half-maximum (fwhm) of ~ 20 nm. The frequency and illumination intensity is controlled by external electronic circuits. The LED bandwidth and light intensity was verified by a commercial silicon PIN photodiode (LSSPD-0.5) with a 3 dB bandwidth of 1 GHz. The results show that the LED can operate properly in a frequency range from 0 to 10 kHz (see data in SI Section 9).

ASSOCIATED CONTENT

Supporting Information

The Supporting Information is available free of charge on the ACS Publications website at DOI: 10.1021/acsnano.8b00004.

Derivation of Hall effect equations; experimental results of bulk silicon photoconductors; additional optoelectronic characteristics for SiNWs; simulation results for SiNWs with fixed charges and/or surface states and LED characteristics (PDF)

AUTHOR INFORMATION

Corresponding Authors

*E-mail: yaping.dan@sjtu.edu.cn.

*E-mail: yongning@mail.xjtu.edu.cn.

ORCID

Yaping Dan: 0000-0002-2983-7213

Notes

The authors declare no competing financial interest.

ACKNOWLEDGMENTS

This work was financially supported by the National Science Foundation of China (61376001) and the Major Research Plan, Science and Technology Commission of Shanghai Municipality (16JC1400405). The nanowire devices were fabricated at the Center for Advanced Electronic Materials and Devices (AEMD), Shanghai Jiao Tong University. Low-temperature Hall effect measurements were conducted at the Instrumental Analysis Center (IAC) of Shanghai Jiao Tong University. The authors thank M. Fanciulli for useful discussions.

REFERENCES

- (1) Choi, D.; Jang, Y.; Lee, J.; Jeong, G. H.; Whang, D.; Hwang, S. W.; Cho, K. S.; Kim, S. W. Diameter-Controlled and Surface-Modified Sb₂Se₃ Nanowires and Their Photodetector Performance. *Sci. Rep.* **2015**, *4*, 6714.
- (2) Kuo, C.-H.; Wu, J.-M.; Lin, S.-J.; Chang, W.-C. High Sensitivity of Middle-Wavelength Infrared Photodetectors Based on an Individual InSb Nanowire. *Nanoscale Res. Lett.* **2013**, *8*, 327.
- (3) Soci, C.; Zhang, A.; Bao, X.-Y.; Kim, H.; Lo, Y.; Wang, D. Nanowire Photodetectors. *J. Nanosci. Nanotechnol.* **2010**, *10*, 1430–1449.

- (4) Neamen, D. A. *Semiconductor Physics and Devices: Basic Principles*, 4th ed.; McGraw-Hill Education: New York, 2011.

- (5) Petritz, R. L. Theory of Photoconductivity in Semiconductor Films. *Phys. Rev.* **1956**, *104*, 1508–1516.

- (6) Matsuo, N.; Ohno, H.; Hasegawa, H. Mechanism of High Gain in GaAs Photoconductive Detectors under Low Excitation. *Jpn. J. Appl. Phys.* **1984**, *23*, L299.

- (7) Zardas, G. E.; Aidinis, C. J.; Anagnostakis, E. A.; Symeonides, C. I. On a Predictive Scheme of Slow Photoconductive Gain Evolution in Epitaxial Layer/Substrate Optoelectronic Nanodevices. *Open J. Microphys.* **2011**, *01*, 32–34.

- (8) Konstantatos, G.; Badioli, M.; Gaudreau, L.; Osmond, J.; Bernechea, M.; Garcia de Arquer, F. P.; Gatti, F.; Koppens, F. H. Hybrid Graphene-Quantum Dot Phototransistors with Ultrahigh Gain. *Nat. Nanotechnol.* **2012**, *7*, 363–368.

- (9) Garrido, J. A.; Monroy, E.; Izpura, I.; Muñoz, E. Photoconductive Gain Modeling of GaN Photodetectors. *Semicond. Sci. Technol.* **1998**, *13*, 563–568.

- (10) Muñoz, E.; Monroy, E.; Garrido, J. A.; Izpura, I.; Sánchez, F. J.; Sánchez-García, M. A.; Calleja, E.; Beaumont, B.; Gibart, P. Photoconductor Gain Mechanisms in GaN Ultraviolet Detectors. *Appl. Phys. Lett.* **1997**, *71*, 870–872.

- (11) Calarco, R.; Marso, M.; Richter, T.; Aykanat, A. I.; Meijers, R.; Hart, A. v. d.; Stoica, T.; Luth, H. Size-Dependent Photoconductivity in MBE-Grown GaN-Nanowires. *Nano Lett.* **2005**, *5*, 981–984.

- (12) Kim, C. J.; Lee, H. S.; Cho, Y. J.; Kang, K.; Jo, M. H. Diameter-Dependent Internal Gain in Ohmic Ge Nanowire Photodetectors. *Nano Lett.* **2010**, *10*, 2043–2048.

- (13) Furchi, M. M.; Polyushkin, D. K.; Pospischil, A.; Mueller, T. Mechanisms of Photoconductivity in Atomically Thin MoS₂. *Nano Lett.* **2014**, *14*, 6165–6170.

- (14) Xu, Q.; Dan, Y. Uncovering the Density of Nanowire Surface Trap States Hidden in the Transient Photoconductance. *Nanoscale* **2016**, *8*, 15934–15938.

- (15) Das, K.; Mukherjee, S.; Manna, S.; Ray, S. K.; Raychaudhuri, A. K. Single Si nanowire (diameter $< \neq 100$ nm) Based Polarization Sensitive Near-Infrared Photodetector with Ultra-High Responsivity. *Nanoscale* **2014**, *6*, 11232–11239.

- (16) Zhang, A.; Kim, H.; Cheng, J.; Lo, Y.-H. Ultra-High Responsivity Visible and Infrared Detection Using Silicon Nanowire Phototransistors. *Nano Lett.* **2010**, *10*, 2117–2120.

- (17) Zhao, X.; Tu, P.; He, J.; Zhu, H.; Dan, Y. Cryogenically Probing the Surface Trap States of Single Nanowires Passivated by Self-Assembled Molecular Monolayers. *Nanoscale* **2018**, *10*, 82–86.

- (18) Dan, Y.; Seo, K.; Takei, K.; Meza, J. H.; Javey, A.; Crozier, K. B. Dramatic Reduction of Surface Recombination by *in situ* Surface Passivation of Silicon Nanowires. *Nano Lett.* **2011**, *11*, 2527–2523.

- (19) Ragnarsson, L.-Å.; Lundgren, P. Electrical Characterization of Pb Centers in (100)Si–SiO₂ Structures: The Influence of Surface Potential on Passivation during Post Metallization Anneal. *J. Appl. Phys.* **2000**, *88*, 938–942.

- (20) Cheng, G.; Wu, X.; Liu, B.; Li, B.; Zhang, X.; Du, Z. ZnO Nanowire Schottky Barrier Ultraviolet Photodetector with High Sensitivity and Fast Recovery Speed. *Appl. Phys. Lett.* **2011**, *99*, 203105.

- (21) Li, Y.; Della Valle, F.; Simonnet, M.; Yamada, I.; Delaunay, J.-J. Competitive Surface Effects of Oxygen and Water on UV Photo-response of ZnO Nanowires. *Appl. Phys. Lett.* **2009**, *94*, 023110.

- (22) Das, S.; Dhyani, V.; Georgiev, Y. M.; Williams, D. A. High Sensitivity Silicon Single Nanowire Junctionless Phototransistor. *Appl. Phys. Lett.* **2016**, *108*, 063113.